PETROLEUM EXPLORATION AND DEVELOPMENT
Volume 53, Issue 1, February 2026
http://www.sciencedirect.com/journal/petroleum-exploration-and-development

Available online at www.sciencedirect.com
ScienceDirect

Cite this article as: PETROL. EXPLOR. DEVELOP., 2026, 53(1): 205–220.

RESEARCH PAPER

Geomodelling of multi-scenario non-stationary reservoirs with enhanced GANSim

SONG Suihong[1, *], MUKERJI Tapan[1], SCHEIDT Celine[1], ALQASSAB Hisham M.[2], FENG Man[2]

1. Department of Energy Science and Engineering, Stanford University, Stanford, CA 94305, USA;
2. ExxonMobil Technology & Engineering Company, Spring, Texas 77389, USA

Abstract: GANSim is a generative adversarial networks (GANs)-based geomodelling framework with direct conditioning capabilities. To extend GANSim for geomodelling of multi-scenario and non-stationary reservoirs, and to address its tendency to overlook single-pixel well facies conditioning data that can cause local facies disconnections around wells, an enhanced GANSim framework is proposed. The effectiveness of the enhanced GANSim is validated using a 3D multi-scenario, non-stationary turbidite fan reservoir. For reservoirs that may involve multiple geological scenarios, two GANSim geomodelling workflows are proposed: (1) training a comprehensive GANSim model that covers all possible geological scenarios; and (2) first performing geological scenario falsification and then training GANSim models only for the unfalsified scenarios. On this basis, a local discriminator architecture is designed to improve facies continuity around wells. The modelling results show that both workflows can generate non-stationary facies models that conform to expected geological patterns and honor conditioning data, and the facies discontinuity issue around wells is effectively resolved. Compared with multipoint geostatistical methods (SNESIM), GANSim exhibits superior capability in reproducing geological patterns and modelling efficiency. Although GANSim requires a long training time, once training is completed, it can be applied to geomodelling reservoirs of arbitrary scale with similar geological structures, achieving modelling speeds approximately 1 000 times faster than SNESIM.

Key words: reservoir geomodelling; generative adversarial networks (GANs); enhanced GANSim; scenario falsification; non-stationary reservoirs; turbidite fan

Introduction

Reservoir geomodelling plays a critical role in various applications, including hydrocarbon exploration, geological storage of CO_2, hydrogen exploration, geothermal energy development, groundwater management, and contamination disposal. Geomodelling is fundamentally a process of integrating diverse sources and forms of data and information, such as geological knowledge, borehole interpretations, geophysical data, and temporal well production data. Despite the availability of these data types, the data are often insufficient to fully capture the complexity, high-dimensionality, and multi-scale nature of subsurface systems. As a result, uncertainty persists even when all collected data sources are effectively integrated. In practice, multiple facies geomodel realizations are produced to represent the uncertainty of subsurface reservoirs, thus providing quantitative and scientific basis for reservoir analysis and decision-making.

Traditionally, geostatistical approaches have been widely used for reservoir facies geomodelling, such as variogram-based methods (e.g., sequential indicator simulation) [1] and multiple-point statistics (MPS) [2]. Variogram-based and MPS methods are effective at honoring well facies interpretations and geophysics-interpreted facies probability cubes. However, these methods often struggle to accurately reproduce complex spatial geological patterns [3]. Recently, deep generative methods have demonstrated strong ability to capture and reproduce complex spatial patterns, e.g., Generative Adversarial Networks (GANs) [4] and diffusion models [5]. GANs, in particular, have been extensively researched and applied in geomodelling [6–13], while diffusion models, despite their potential, are still in the early research stage for geomodelling [14–16].

In GANs, the generator maps a latent vector to an output, while the discriminator distinguishes between

Received date: 24 Aug. 2025; **Revised date:** 19 Jan. 2026.
*** Corresponding author.** E-mail: suihong@stanford.edu
https://doi.org/10.1016/S1876-3804(26)60685-4

real and generated data. Through alternative training of the discriminator and generator, the generator eventually learns and can reproduce complete spatial patterns exhibited in the training dataset. When applied to geomodelling, the generator learns geological patterns from training conceptual geomodels which are constructed based on geological knowledge, and can then generate reservoir geomodels that exhibit the learned patterns [6, 17–18]. However, vanilla GANs alone do not provide conditioning for geomodelling. To address this, post-GANs latent vector perturbation workflows have been proposed. These workflows search for appropriate latent vectors that, when fed into a pre-trained generator, produce geomodel realizations that are both realistic and consistent with given conditioning data [6, 17, 19–21]. Such latent vector search methods can include Markov chain Monte Carlo (McMC) [22], iterative ensemble smoother (IES) [23], and gradient-based optimization techniques. However, once the conditioning data changes, the latent vector search process must be repeated, which is computationally expensive. Additionally, 100% conditioning accuracy cannot always be guaranteed for well facies data.

Therefore, Song et al. [24–25] proposed GANSim, a GANs-based geomodelling workflow, for reservoir geomodelling directly conditioned on well facies data, geophysically interpreted facies probability cubes, and global features such as facies proportions. In GANSim, in addition to the original adversarial loss, condition-based loss functions are introduced to train the generator to learn both conditioning rules (i.e., the relationship between output facies models and input conditioning data) and geological patterns. With these two types of learned knowledge, the trained generator can quickly produce multiple realistic and conditional facies model realizations for any given conditioning data. Furthermore, due to the fully convolutional design of the generator architecture, although trained on smaller-scale conceptual geomodels or their patches, the generator can produce reservoir geomodel realizations of arbitrarily large scales once trained. GANSim has been successfully applied for conditional geomodelling of 3D field karst cave reservoirs [8] and meandering channel reservoirs [26]. Similarly to GANSim, Cui et al. [12] also proposed a multiple-condition fusion network combined with GANs for direct geomodelling conditioned on both hard and soft data. To incorporate well production data, Song et al. [9] further proposed a GANSim-surrogate framework. In this framework, a deep learning-based surrogate model is trained in conjunction with the pre-trained generator, and appropriate input latent vectors are searched so that the output facies geomodels are consistent with the given production data (through the trained surrogate) as well as the given well facies interpretations, facies probability maps, and global feature values. To efficiently construct such a surrogate, a purely physics-informed neural operator approach can be employed [27].

However, the proposed GANSim workflow and its field applications still have limitations. First, in previous algorithm development research and field applications [8, 24–26], GANSim has primarily been used for single-scenario reservoirs, i.e., reservoirs exhibiting unimodal distribution in geological pattern uncertainty. However, in reality, due to limited knowledge of the subsurface, the assumed reservoir scenarios can be diverse (scenario uncertainty). For example, in the case of a channel reservoir, the assumed geological scenarios may include meandering channels, braided channels, and a transitional form between them. Similarly, delta reservoirs may involve scenarios such as the jet-plume model [28] as well as the classic model comprising a delta plain, delta front, and pro-delta. Turbidite reservoirs may involve scenarios with varying levels of confinement [29]. Given this diversity of possible geological scenarios, how can GANSim be adapted for geomodelling of such common multi-scenario reservoirs?

Secondly, due to computational resource limitations, large-size conceptual geomodels are commonly cropped into smaller-size patches for training GANSim. As a result, the generator learns pattern fragments from these smaller conceptual geomodel patches. When applied to geomodelling of large-size reservoirs, the trained generator essentially samples the learned pattern fragments for different locations within the reservoir domain. This approach is theoretically reasonable and has proven successful in cases where the spatial patterns are statistically stationary, such as karst cave and meandering channel reservoirs [8, 26]. It works because pattern fragments across the entire reservoir domain are similar (from the same distribution) in stationary cases, and there is no strict ordering requirement for pattern fragments at different locations during generation. However, for non-stationary reservoirs, the pattern fragments vary significantly across the entire domain, and there is an implicit ordering requirement for local patterns at different locations. In this case, if GANSim is still trained with conceptual geomodel patches, the generated large-size reservoir geomodels may exhibit significant disorganization of patterns. For example, a proximal delta pattern might directly connect to a distal delta pattern without a transitional medial pattern. In the current GANSim algorithm, the conditioning on facies probability cubes and maps of global features is considered [3], which might guide the generator to sample appropriate pattern fragments for different locations during geomodelling. In this sense, the trained generator may still produce well-organized non-stationary geological patterns. However, this requires verification with non-stationary complex 3D reservoir cases.

Thirdly, a persistent challenge in current GANSim implementations is the discriminator's tendency to overlook

single-pixel (single-voxel) well facies data, leading to severe disconnections between the single-pixel well facies data and surrounding geobodies of the same facies type in a generated realization [24]. To mitigate this, studies have artificially expanded well facies into multi-pixel blocks (e.g., 4×4 pixels [8, 24]). However, this deliberate expansion of well facies introduces local unrealistic artifacts around the wells and artificially reduces the local reservoir prediction uncertainty. Is it possible to improve GANSim so that the original single-pixel well facies data are not overlooked by the discriminator, eliminating the need for deliberate well facies expansion? Solving this challenge is crucial for all GANSim applications, regardless of reservoir scenario uncertainty (single vs. multi-scenario) and spatial pattern types (stationary vs. non-stationary).

In this paper, we enhance GANSim by proposing two workflows for reservoirs with multiple possible scenarios and by introducing a local discriminator design to address the local disconnection problem around well facies data (Section 1). In Section 2, a multi-scenario, non-stationary 3D turbidite fan reservoir is used as an example to validate the effectiveness of the enhanced GANSim and to demonstrate its reliability for modelling 3D non-stationary reservoirs. Finally, discussions and conclusions are presented in Sections 3 and 4, respectively.

1. Enhanced GANSim

1.1. Two GANSim workflows for multi-scenario reservoirs

We propose two GANSim geomodelling workflows for reservoirs with geological scenario uncertainty. The major steps of the first workflow are as follows:

(1) Geological knowledge compilation for different scenarios: Compile geological knowledge for each possible geological scenario. This may include variations in geometrical shapes and topological relationships of reservoir geobodies, variations in sedimentary facies, reservoir formation processes, and the dimensional ranges of geobodies.

(2) Creation of conceptual geomodels for each scenario: The complied geological knowledge is conceptualized into computer-readable formats such as logical rules, mathematical equations, and maps. Automated workflows are then developed based on this conceptualized knowledge to efficiently emulate conceptual geomodels for different scenarios. These workflows may be physics-based, process-mimicking, or object-based, depending on the desired balance between geological realism and computational efficiency [30].

(3) Prior falsification using observed data: Due to insufficient understanding and inaccuracies during the compilation of geological knowledge and creation of conceptual goemodels, the emulated conceptual geomodels may not reflect the uncertainty of real subsurface reservoir distribution. Thus, the ensemble of conceptual geomodels of all scenarios are combined (collectively referred to as the prior) to go through a prior falsification process using observed actual conditioning data. If this prior ensemble is falsified, the geological knowledge and/or the conceptual geomodel emulation workflow are continuously refined until the prior ensemble can no longer be falsified. Section 1.2 provides more details on the prior falsification process.

(4) Building the training dataset for GANSim: The training dataset includes diverse conceptual geomodels of all scenarios as well as their well facies data and facies probability cubes. To reduce the training burden, large-size conceptual geomodels are typically cropped into smaller-size patches, from which the training well facies and probability cubes can be obtained. The crop size represents a trade-off between training efficiency and the geological realism of the generated models [8].

(5) Design of neural network architectures for the generator and discriminator in GANSim: The generator and discriminator architectures are enhanced compared to the previous version of GANSim, as described in Section 1.3.

(6) Training of GANSim: A single GANSim model is trained for all scenarios using the training dataset and the loss functions described in Section 1.3.

(7) Evaluation of the trained generator: The generator is evaluated based on its ability to reproduce expected geological patterns, its conditioning capability, and the variety of the produced geomodels. Evaluation methods include visual inspection, multidimensional scaling (MDS), and other techniques [25].

(8) Geomodelling for large field reservoirs: The trained generator is used to model arbitrarily large field reservoirs by taking in field conditioning data and varying expanded latent cubes. This enables generation of multiple conditional realizations, which are then assessed for geological realism, conditioning accuracy, and the variety of the produced geomodels.

The second workflow is largely similar to the first workflow, with the key difference that, in workflow 2, an additional geological scenario falsification process using conditioning data is introduced after the prior falsification step. Then, for each unfalsified geological scenario, a training dataset is constructed, the neural network architectures of the generator and discriminator are enhanced, and a specialized GANSim model is trained. The trained generator is then evaluated and finally applied to geomodelling of field-scale reservoirs only for that specific unfalsified scenario. Section 1.2 provides more details on the scenario falsification steps.

In the first workflow, multiple geological scenarios are combined to train a single comprehensive generator. This

generator simultaneously learns geological knowledge across all scenarios as well as conditioning rules (i.e., the relationships between output facies models and input conditioning data), enabling it to be applied to geomodelling under different geological scenarios. Compared with the first workflow, the generators obtained in the second workflow are only applicable to their corresponding unfalsified scenarios, but they are generally easier to train than the comprehensive generator in the first workflow.

1.2. Prior and geological scenario falsification process

In this study, the term prior refers to the ensemble of all geological scenarios or their conceptual geomodels and can be viewed as a "super scenario", so the prior falsification is actually a special case of the scenario falsification. In the following, we describe the scenario falsification process, which also applies to prior falsification.

The idea of falsification in science is not new [31] and has been applied across various scientific domains, including geosciences [32–33]. A simple interpretation of the logic behind reservoir scenario falsification is as follows: if the actual subsurface reservoir distribution belongs to a certain geological scenario, then the ground truth geomodel describing the actual reservoir distribution lies within the range of all conceptual geomodels emulated based on the geological knowledge of that scenario; consequently, the observed data (e.g., geophysical data) from the actual reservoir will also lie within the range of the data forward-simulated from these conceptual geomodels, both in the original data space and in any reduced data feature space. Conversely, if the observed data does not lie within the simulated data range in the original or any reduced feature space, then the actual reservoir does not belong to the scenario and the scenario is therefore falsified.

The common steps of scenario falsification involve generating a number of conceptual geomodels for each scenario, forward-simulating these conceptual geomodels to obtain corresponding data, extracting sensitive features from both the simulated data and the observed data, and projecting these data (simulated and observed) into a low-dimensional space using the Multidimensional Scaling (MDS) method [34] based on the feature distance of every pair of data. Finally, the posterior probability of the scenarios given the features of the observed data (see Eq. (1) below) is evaluated in the low-dimensional MDS space to determine whether the scenario is falsified. The posterior probability of each scenario is calculated as

$$P\left[S_k \middle| f(\boldsymbol{d})\right] \approx \frac{P\left[f(\boldsymbol{d})|S_k\right]P(S_k)}{\sum_k P\left[f(\boldsymbol{d})|S_k\right]P(S_k)} \tag{1}$$

where, S_k represents the k-th scenario ($1 \le k \le K$), $f(\boldsymbol{d})$ represents the sensitive feature of the observed data $\boldsymbol{d}$. $P(S_k)$ is the prior probability of S_k. The likelihood $P[f(\boldsymbol{d})|S_k]$ is evaluated based on the probability density at the feature point of the observed data in the MDS space [35]. The "≈" symbol is used in the equation because the likelihood is evaluated in a low-dimensional MDS space rather than the original feature space, and it also accounts for all inaccuracies involved in the conceptual geomodel generation and forward simulation. Note that the evaluated $P[S_k|f(\boldsymbol{d})]$ differs from the posterior $P(S_k|\boldsymbol{d})$ obtained from inversion processes, as only partial information of the observed data (i.e., its global statistical features $f(\boldsymbol{d})$) is used for conditioning here in the falsification process. Uncertainty in the forward simulation, such as uncertainty in the rock physics model for seismic data, should also be considered. The feature filter function, $f(\cdot)$, should be sensitive to geological scenarios.

The data $\boldsymbol{d}$ can be any observed data type related to reservoir facies geomodel, including flow simulation data [36], well facies data [35], seismic data [37], or electrical resistivity tomography [38]. In this paper, we consider well facies interpretations at different locations and seismic data as $\boldsymbol{d}$. For well facies interpretations, the multi-point histogram analysis is used as the feature filter function to extract facies stacking patterns along well profiles [35, 39]. For seismic data, a 2D discrete wavelet transform approach is used as the feature filter function to extract the spatial patterns of seismic data which is informative for geological scenarios [37]. Due to the potential information redundancy between the two posteriors conditioned on the sensitive features of the observed well facies and seismic data, a probability combination scheme commonly used in geostatistics, the Tau model [40], is used to obtain the joint posterior of each scenario, based on which scenarios with low posterior values are falsified.

In addition to reservoir prediction, the falsification process is also widely used in the construction of mineral geomodels. For example, Wei et al. [41] integrated falsification into a geophysical inversion workflow for a 3D real case constrained by soil geochemistry, borehole data, and airborne geophysical observations.

For prior falsification, the hypothesis to be tested becomes that "the actual reservoir belongs to the prior ensemble of all scenarios." Using the same work steps as in scenario falsification, the posterior probability of this hypothesis, conditioned on sensitive features of the given observational data, is calculated. If the posterior probability is lower than a predefined threshold, the hypothesis is falsified under the sensitive features of the current observational constraints.

1.3. Local discriminator design

In the earlier GANSim implementation, the discriminator primarily focuses on assessing the global geological realism of the entire reservoir geomodel and often over-

looks the sparsely distributed single-pixel well facies data, leading to significant disconnections between the input well facies pixels and the surrounding geobodies of the same facies type in geomodels produced by the generator. This local disconnection issue significantly affects flow behaviors of the generated reservoir geomodels. To address this limitation, we propose to design local discriminators that specifically evaluate and finally can improve the local geological realism around well facies data, in addition to the original global discriminator. Multiple local discriminators can be designed to focus on different scales of locality around wells. These local discriminators can either be separate from or integrated into the global discriminator. In the integrated design, local discriminators share the same shallow convolutional layers with the global one. Our experiments show that both separate and integrated architectures produce similar results. Fig. 1 shows an example of the integrated discriminator design. Note the well location indicator cube is considered as another input of the discriminator for easier calculation of local discriminator scores.

The Wasserstein loss function with gradient penalty [42] is used in GANSim. We found that the generator achieves good local and global realism by summing up the Wasserstein losses of global and local discriminators, rather than summing their scores first and then calculating a single Wasserstein loss. Appropriate weights are assigned to the Wasserstein losses of these discriminators during the summation. With this local discriminator design, the well facies data expansion approach [8, 24] is no longer necessary, thereby alleviating artifacts associated with expanded well facies data.

With local discriminator design, the loss function of the generator becomes:

$$L(G)=\mathbb{E}_{\boldsymbol{z}\sim p(\boldsymbol{z}),(\boldsymbol{w},\boldsymbol{\pi})\sim p(\boldsymbol{w},\boldsymbol{\pi})}\sum_{i=0}^{n}-\alpha_i D_i\left[G(\boldsymbol{z},\boldsymbol{w},\boldsymbol{\pi}),I_{\mathrm{wl}}(\boldsymbol{w})\right]+\beta_1 L_{\mathrm{w}}\left[G(\boldsymbol{z},\boldsymbol{w},\boldsymbol{\pi}),\boldsymbol{w}\right]+\beta_2 L_{\pi}\left[G(\boldsymbol{z},\boldsymbol{w},\boldsymbol{\pi}),\boldsymbol{\pi}\right] \quad (2)$$

where, G refers to the generator, D_0, D_1, …, D_n represent the global discriminator (D_0) and n local discriminators respectively, α_i are the corresponding weights for each discriminator; $\boldsymbol{z}$, $\boldsymbol{w}$, and $\boldsymbol{\pi}$ refer to the input latent vector, input training well facies data, and input training probability maps or cubes, $p(\boldsymbol{z})$ and $p(\boldsymbol{w},\boldsymbol{\pi})$ are the distribution of the latent vector and the distribution of the training well and probability data; I_{wl} is a function to extract well location indicator from training well facies data $\boldsymbol{w}$; L_{w} and L_{π} are the condition loss terms for well facies and probability cubes, β_1 and β_2 are their respective weights, and $\mathbb{E}$ is the expectation operator. The discriminator loss is defined as

$$L(D)=\mathbb{E}_{\boldsymbol{z}\sim p(\boldsymbol{z}),(\boldsymbol{w},\boldsymbol{\pi})\sim p(\boldsymbol{w},\boldsymbol{\pi}),\boldsymbol{x}\sim p(\boldsymbol{x})}\sum_{i=0}^{n}\alpha_i\left\{D_i\left[G(\boldsymbol{z},\boldsymbol{w},\boldsymbol{\pi}),I_{\mathrm{wl}}(\boldsymbol{w})\right]-D_i\left[\boldsymbol{x},I_{\mathrm{wl}}(\boldsymbol{w})\right]+\lambda\mathbb{E}\left[\|\nabla_{\hat{\boldsymbol{x}}}D_i(\hat{\boldsymbol{x}},I_{\mathrm{wl}}(\boldsymbol{w}))\|_2-1\right]^2\right\} \quad (3)$$

where, $\boldsymbol{x}$ refers to a training facies model and $p(\boldsymbol{x})$ is its distribution, $\hat{\boldsymbol{x}}$ is sampled between an $\boldsymbol{x}$ and an $\boldsymbol{x}_{\mathrm{G}}=G(\boldsymbol{z},\boldsymbol{w},\boldsymbol{\pi})$, i.e., $\hat{\boldsymbol{x}}=t\boldsymbol{x}+(1-t)\boldsymbol{x}_{\mathrm{G}}$, with t~Uniform (0, 1), and λ is a predefined weight for gradient penalty. Global feature conditioning is not explicitly included in the above loss functions. To incorporate global features, the corresponding loss terms can be directly added to the above generator loss (Eq. (2)) [3, 24].

To improve the reasonability of the neural network architectures in GANSim, we further revised the generator's output and the discriminator's input from a single facies geomodel to multiple facies indicator models (i.e., "one-hot" encoding of facies categories) of all facies types (Fig. 1). During geomodelling for field reservoirs, these facies indicators are converted into a reservoir facies model using argmax or thresholding-related operations. This design is common in variogram-based facies geomodelling algorithms, such as sequential indicator simulation [1].

Fig. 1 illustrates the enhanced architecture of the generator and discriminator used for facies geomodelling of turbidite fan reservoirs in this study. The turbidite fan reservoir has three facies categories: channels, lobes, and background mud. The generator takes as inputs 8 latent cubes with a size of 4×4×4, 2 well facies cubes each with a size of 128×128×32 representing a well facies code cube and a well location indicator cube, and 2 probability cubes with a size of 128×128×32 for channel and lobe facies. The output of the generator includes three facies indicator cubes for channel, lobe, and mud facies, respectively, each with a size of 128×128×32. The generator employs a fully convolutional layer design, enabling geomodelling of arbitrarily large reservoirs by the generator after training. This approach is not constrained by the size of the training geomodel patches [8]. ReLU activation functions are used for all layers of the generator except the last one, which utilizes a softmax activation function.

For the discriminator, the inputs consist of three facies indicator cubes and one well location indicator cube, each with a size of 128×128×32. The architecture includes one global discriminator and three local discriminators. The global discriminator processes the inputs with several convolutional, downsampling, minibatch standard deviation, and fully connected layers, and finally produces a score representing the global realism of the input facies indicators (the backbone neural layers of Fig. 1b). The local discriminator shares the same inputs and the first several convolutional and downsampling layers with the global discriminator (e.g., the backbone neural layers before the data cube of 64×64×16 for local discriminator 1 in Fig. 1b). Then, several separate convolutional layers with the kernel size of 3×3×1 and 1×1×1 (convolutional layer b and c in Fig. 1b) follow to produce a small feature cube (e.g., the data cube with a size of 64×64×16 after convolutional layer b and c in local discriminator 1).

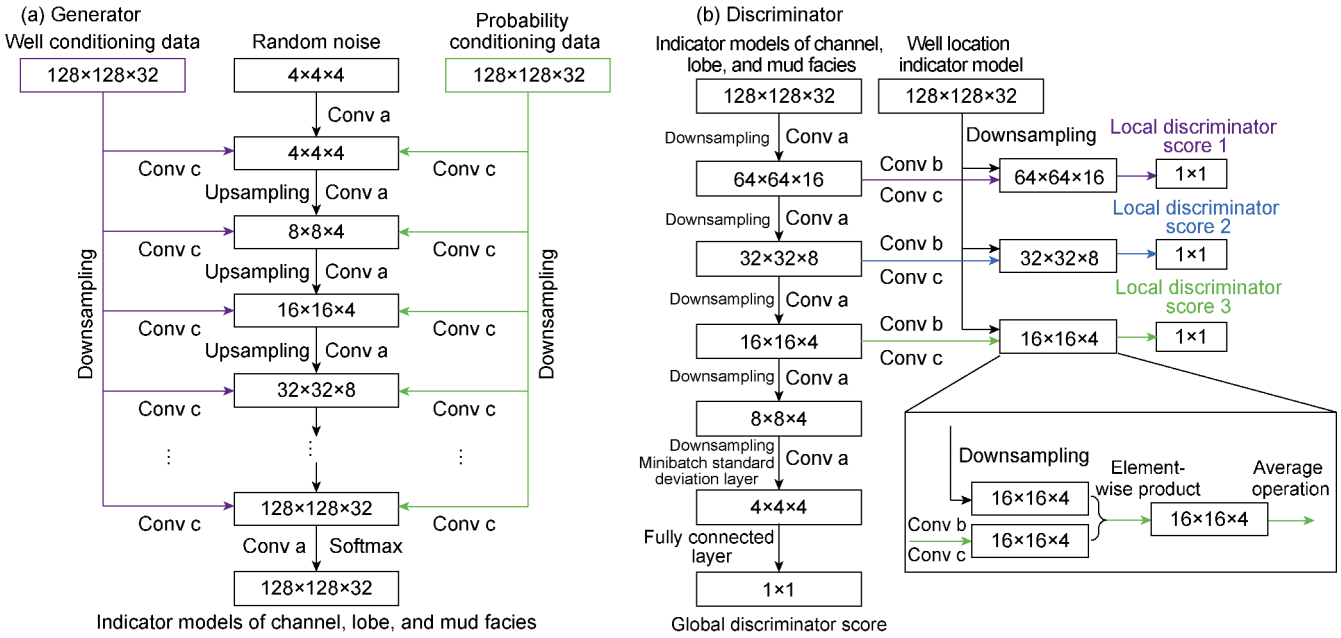

Fig. 1. The generator and discriminator architectures used for geomodelling of turbidite fan reservoir in this study. The global and local discriminators adopt an integrated architectural design; Conv a/b/c refers to convolutional layers with the kernel size of 3×3×3/3×3×1/1×1×1.

Each feature value in the feature cube corresponds to a receptive field — that is, a localized region of the input facies indicator cubes contributing to the feature value— and reflects the realism of that region. An element-wise multiplication is then performed between this feature cube and a downsampled well location indicator cube of the same size, effectively masking the feature cube to only focus on receptive fields near wells. The result is then averaged to compute a local score, which quantifies the local realism within receptive fields around all wells in the input facies indicator cubes. The size of the receptive fields can be analytically derived from the convolution and downsampling operations from the input facies indicators to the feature cube. Local discriminator 1 evaluates the realism within a local region of 18×18×14 cells (receptive size of the local discriminator score 1) around all wells, while local discriminator 2 corresponds to a locality of 40×40×32 cells, and local discriminator 3 corresponds to a locality of 84×84×32 cells around all wells. Since the Wasserstein loss is used, the final layer of the discriminator employs a linear activation function, while ReLU is used for all other layers.

2. Application of enhanced GANSim to geomodelling of multi-scenario non-stationary turbidite fan reservoirs

Turbidite fan reservoirs are high-quality reservoirs for hydrocarbon accumulation, carbon dioxide sequestration, and groundwater storage. They mainly consist of submarine turbidite channels, lobes, and background mudstones, among which the former two constitute the primary storage space. Both channels and lobes exhibit divergent distribution features from the sediment source toward the distal area, showing typical non-stationary characteristics. Because the development of turbidite channels can be constrained to different degrees [29, 43, 44], turbidite fan reservoirs can be summarized into five geological scenarios: (1) strongly confined channels and lobes (channels are strictly confined, and different stages of channels are almost vertically stacked), (2) a transitional scenario between strongly confined and valley-confined scenario, (3) valley-confined channels and lobes (channels are restricted within valleys), (4) weakly confined channels and lobes (channels experience relatively low degrees of confinement), and (5) unconfined channels and lobes (channels develop without spatial confinement). In each scenario, lobe deposits may be eroded by later channel infilling. The coexistence of geological scenario uncertainty and non-stationary characteristics makes turbidite fan reservoirs an ideal validation case for enhanced GANSim geomodelling framework.

Based on the geological characteristics of turbidite fan reservoirs, this study proposes an object-based three-dimensional conceptual geomodel emulation workflow in Petrel. The key steps include: (1) constructing a probability map of channel endpoints, (2) randomly sampling a specified number of channel endpoints from the probability map, (3) simulating channels from endpoints toward the sediment source, (4) simulating lobes, and (5) integrating the simulated channel and lobe geobodies. By adjusting the distribution of the channel-endpoint probability map and the sampling number of channel endpoints, conceptual geomodels corresponding to the five geological scenarios can be emulated. It should be noted

that this emulation workflow cannot fully incorporate conditioning data such as well facies interpretations. Using this workflow, a turbidite fan reservoir geomodel under the strongly confined scenario is simulated as a reference ground truth geomodel (Fig. 2a), and the corresponding reservoir is referred to as the reference reservoir in this paper. The ground truth geomodel contains 400 × 400 × 100 grid cells, with a cell size of 50 m × 50 m × 0.5 m. Eighteen wells are then randomly extracted from the ground truth geomodel to obtain the well facies interpretations. The three-dimensional seismic data is forward simulated from the ground truth geomodel. In addition, Gaussian smoothing is applied to the facies indicator models of the ground truth geomodel to obtain probability cubes of channels and lobes, which are similar to the results derived from geophysical interpretation [45]. Fig. 2b–2d show these observational data about the reference reservoir. In the following sections, without assuming knowledge of the distribution of the reference reservoir (i.e., the ground truth geomodel), we use the above well facies interpretations, seismic data, and facies probability cubes as conditioning data, together with general geological knowledge of turbidite fan reservoirs, to model the possible distribution of the reference reservoir using enhanced GANSim.

2.1. Geomodelling of turbidite fan reservoir with GANSim workflow 1

The first step in the GANSim workflow 1 is the compilation of geological knowledge about the target reservoir, with particular attention to different possible scenarios. The geological knowledge of the five turbidite fan reservoir scenarios has been briefly introduced above. The remaining steps of the workflow are described in the following sections.

2.1.1. Construction of conceptual geomodels and the training dataset

We apply the aforementioned object-based workflow to emulate 640 large-scale conceptual geomodel realizations for each of the five geological scenarios. Fig. 3 displays a random conceptual geomodel example for each scenario. Each conceptual geomodel consists of 400×400×50 cells, with cell dimensions of 50 m×50 m×0.5 m.

Following step 3 of GANSim workflow 1, these prior conceptual geomodels should be validated through a prior falsification process using the given conditioning data of the reference reservoir. However, in this synthetic study, since the conceptual geomodels are emulated using the same procedures as the ground truth geomodel, these prior conceptual geomodels of all scenarios, as a whole, would not be falsified by the conditioning data. Therefore, we skip step 3 and proceed directly to preparing the training dataset. Note that in GANSim workflow 2, the scenario falsification process is carried out after this step, as described later in Section 2.2.

To save computational resources, the emulated conceptual geomodels are randomly cropped along channels and lobes to form smaller-size training facies model patches. According to Song et al. [8], for stationary reservoirs, a rule of thumb for the crop size is that it should be larger than the largest repetitive pattern unit, such as a meander

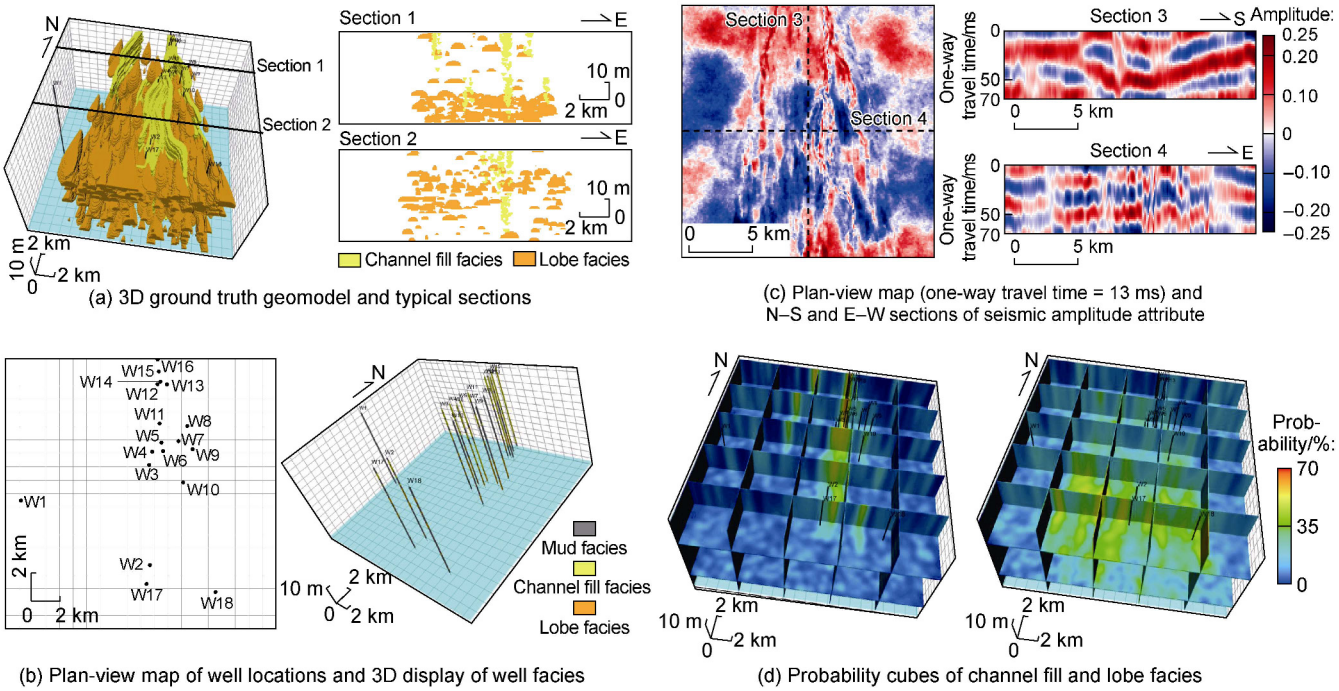

Fig. 2. Ground truth geomodel of the reference reservoir and the corresponding conditioning data (the background mudstone facies in the ground truth geomodel and cross sections are hidden for clarity).

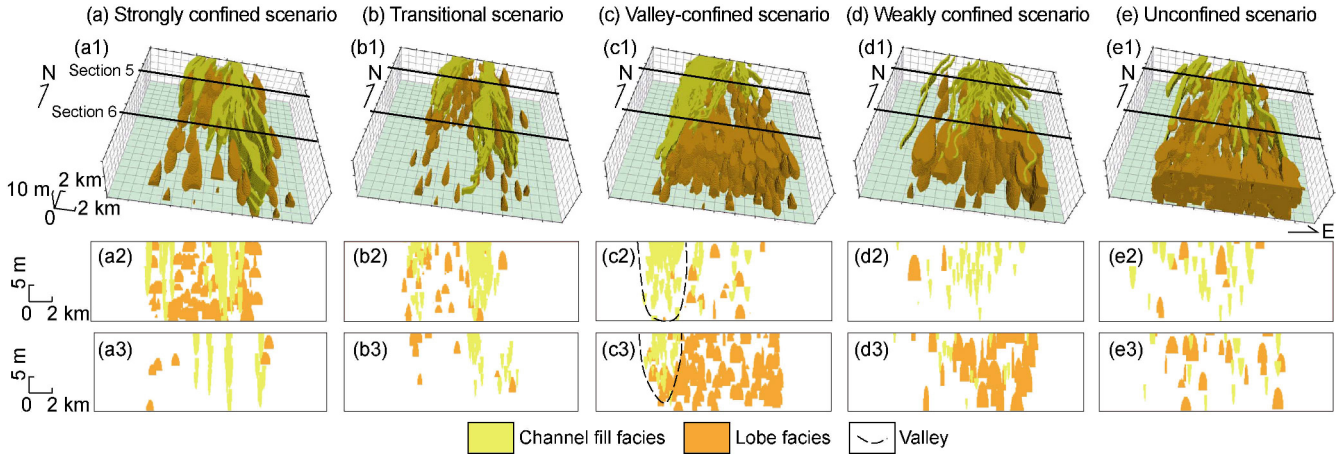

Fig. 3. Examples of conceptual geomodels corresponding to the five turbidite fan reservoir scenarios. Subfigures (a1)–(e1) show 3D conceptual geomodel examples of the five scenarios; subfigures (a2)–(e2) show facies distributions along section 5 of the five conceptual geomodel examples; and subfigures (a3)–(e3) show facies distributions along section 6 of the five conceptual geomodel examples. For better visualization, the background mudstone facies are set to be invisible.

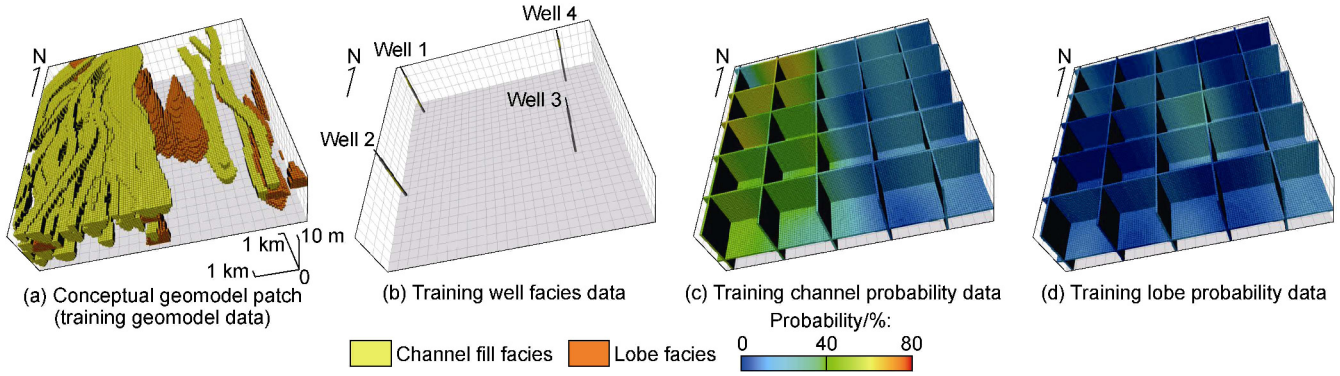

Fig. 4. One random example of training conceptual facies model patches and the corresponding training well facies data and training probability cubes of channels and lobes.

in a meandering channel reservoir. In this non-stationary reservoir study, we maximize the crop size to 128×128×32 cells within the limits of GPU memory resources (during training) to enable the generator to learn as complete non-stationary geological patterns as possible. Finally, 38 400 cropped facies model patches are obtained (12 from each conceptual geomodel), with 35 000 used as training facies models and the remaining reserved for test. Because the progressive training technique [46] is applied in GANSim, these facies model patches are further downsampled to coarser resolutions from 64×64×16, 32×32×8, ..., to 4×4×4. Since facies indicator models are required for training, we further decompose these patches of different resolutions, into indicator models of channel, lobe, and mud facies. From each facies model patch of the finest resolution (128×128×32), we randomly sample 1 to 10 vertical wells—each occupying 1×1 cell horizontally—as the training well facies data. The Gaussian smoothing method, with added noise, is applied to the decomposed indicator patches of the finest resolution to mimic geophysically interpreted probability cubes of channels and lobes, following a similar approach to that of Song et al. [8]. One example of training facies model patches and the corresponding training well facies data and facies probability cubes are shown in Fig. 4.

2.1.2. Neural network architecture design, training, and evaluation of GANSim

The neural network architectures of the generator and discriminator are described in Section 1.3.

We use the minibatch gradient descent method and the Adam optimizer with default parameters [47] for training. The minibatch size is set to 128, which is appropriate for the available GPU memory. Since a progressive training approach is used in GANSim, the layers of the generator and the discriminator are trained progressively from shallow to deep. The generator and discriminator are alternately trained, each with a single minibatch. The weights for the condition-based loss terms of well facies and probability cubes in Eq. (2) (β_1 and β_2) are set as 2 and 0.08, respectively, after trial-and-error experiments. There are one global discriminator and three local discriminators (Fig. 1). Their weights in the loss function (i.e., α_0, α_3, α_2, and α_1 in Eq. (2) and Eq. (3)) are set as 0.1, 0.9, 9, and 90 for the global discriminator, local discriminator 3, local discriminator 2, and local discriminator 1, respectively. The weight λ in Eq. (3) is set as 10 by default. The enhanced GANSim is trained

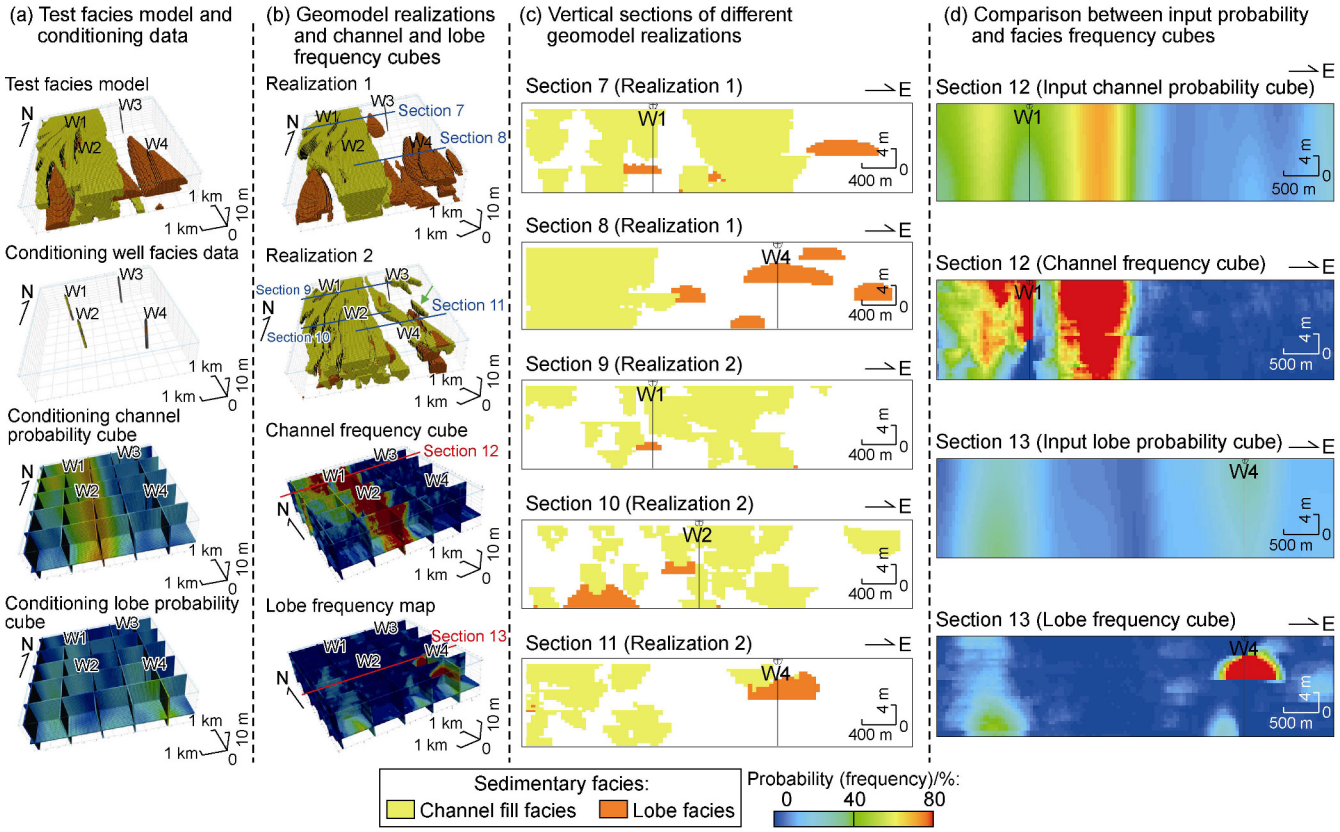

Fig. 5. Evaluation of the generator using one test facies model.

on 8 GPUs (A100-40G) in parallel for 72 h.

After training, we evaluate the generator using different test facies model patches. Fig. 5 shows the evaluation results of one test facies model patch. The conditioning well facies interpretations (128×128×32) and probability cubes of channels and lobes (128×128×32) are taken into the trained generator, along with random latent cubes, to produce different facies model realizations (128×128×32). Each realization takes an average of 0.02 s on one GPU (A100).

From the generated realizations and their cross-sections in Fig. 5, we observe that most of the simulated channels are connected (although a few disconnected channels are present, e.g., the channel patch indicated by the green arrow in realization 2 of Fig. 5) and exhibit a downward concave shape. The simulated lobes show the expected fan-like upward concave shape. The channels may cut through lobes. These features align with the geological knowledge of turbidite fan reservoirs. In addition to the geological realism of the produced geomodels, we calculated the well facies reproduction accuracies, which are almost 100% for all test cases. Frequency cubes of channels and lobes were calculated based on 100 randomly generated geomodel realizations. From a comparison among the geomodel realizations, the calculated facies frequency cubes, and the input facies probability cubes in 3D or 2D views, we observe a distinct consistency between the generated channels and lobes and the input probability cubes of the two facies, indicating a clear conditioning effect of the input probability cubes. Compared with the input probability cubes, the high-value zones in the frequency cube are more concentrated. This behavior is expected and will be discussed in detail in Section 3.1. In addition, the generated geomodel realizations show large variability, which can largely represent the uncertainty in reservoir prediction.

When comparing the generated realizations with and without (Fig. 6) the proposed local discriminator design, unrealistic disconnection artifacts are clearly visible in the cross-well sections of the latter case (highlighted by blue circles in Fig. 6). In contrast, such artifacts are not observed in cases with local discriminators (Fig. 5), demonstrating the effectiveness of the local discriminator design.

In summary, the trained generator can efficiently produce multiple, realistic, and conditional facies model realizations.

2.1.3. Geomodelling for the reference reservoir

After evaluation, the trained generator is used for geomodelling of the reference reservoir assuming that its ground truth facies model is unknown. Note that the reference reservoir, with dimensions of 400×400×100 cells, is over 30 times larger than the training facies model patches, which have dimensions of 128×128×32 cells. The conditioning well facies interpretations and probability cubes of channels and lobes of the reference

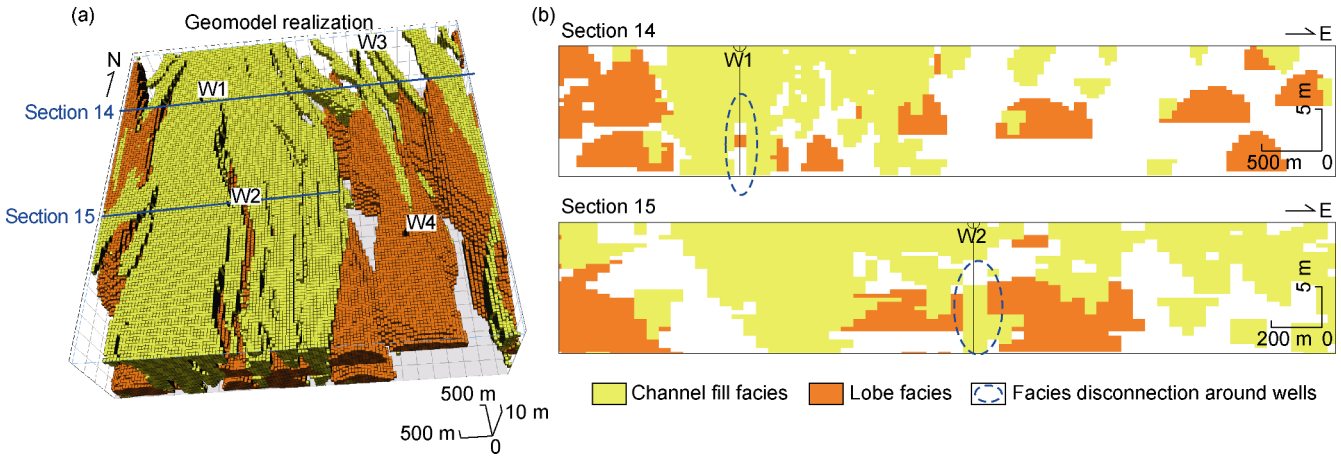

Fig. 6. Random geological realization generated by GANSim without local discriminator design (a) and its cross sections (b) (using the same conditioning data as in Fig. 5).

reservoir as well as random expanded latent cubes are taken as inputs into the trained generator to produce different facies model realizations with a size of 400×400×100. Fig. 7a shows two random geomodel realizations, and Fig. 8a ② shows a cross-well section of one realization (the section is marked as section 16 in Fig. 7a).

2.2. Geomodelling of turbidite fan reservoir with GANSim workflow 2

Unlike GANSim workflow 1, in workflow 2, after prior falsification, a geological scenario falsification process is performed to test the five scenarios using the given conditioning well facies and seismic data, based on the procedures outlined in Section 1.2. Then, for each unfalsified scenario, a GANSim model is trained, and the trained generator is used for geomodelling of the reference reservoir.

2.2.1. Falsification of the five geological scenarios

Since the conceptual geomodels (25 m thick) are half the thickness of the reference reservoir (50 m thick), two conceptual geomodels of the same scenario are stacked to match the thickness of the reference reservoir. Subsequently, 120 stacked conceptual geomodels are randomly selected from each geological scenario. We sample well facies profiles from these stacked conceptual geomodels using the same well locations as those of the reference conditioning wells, and use them as simulated data. Following the procedure described in Section 1.2, and using the conditioning well data of the reference reservoir as observations, the posterior probabilities of the five geological scenarios based on well observations are calculated. From the strongly confined to the unconfined scenarios, the posterior probabilities are 0.41, 0.56, 0.01, 0.02, and 0, respectively. Similarly, seismic data are forward simulated from these stacked conceptual geomodels as simulated data, and the posterior probabilities of the five geological scenarios based on the given seismic data of the reference reservoir are calculated. From the strongly confined to the unconfined scenarios, the posterior probabilities are 0.32, 0.18, 0.25, 0.17, and 0.08, respectively. Finally, the two sets of posterior probabilities are fused using the Tau model, yielding joint posterior probabilities of 0.51, 0.47, 0.01, 0.01, and 0 for the strongly confined to the unconfined scenarios. Accordingly, the last three geological scenarios with very low joint posterior probabilities are falsified, and only the strongly confined and transitional scenarios are retained.

2.2.2. GANSim training and geomodelling for unfalsified scenarios

We train a GANSim model for each of the two unfalsified scenarios using the corresponding training datasets prepared in Section 2.1.1. The GANSim network architectures and other hyperparameter settings are the same as those in the workflow 1. Training the generator for each scenario takes 72 h on 8 GPUs (A100-40G) in parallel.

After evaluating the trained generators, we take as inputs the conditioning data of the reference reservoir into the generators corresponding to the strongly confined and transitional scenarios to generate multiple geomodel realizations. Fig. 7b and 7c show two random geomodel realizations for each of the two unfalsified scenarios. Fig. 8a ③–④ shows a cross-well section of one realization of each scenario, with the section locations marked in Fig. 7a.

3. Geomodelling results analyses and discussions

3.1. GANSim results analyses

Both GANSim workflows achieve 100% accuracy in reproducing the conditioning well facies data. For workflow 1 and the two unfalsified scenarios in workflow 2, 50 geomodel realizations are randomly selected to calculate the frequency cubes of channel and lobe facies (Figs. 7 and 8). The simulated channels and lobes are consistent

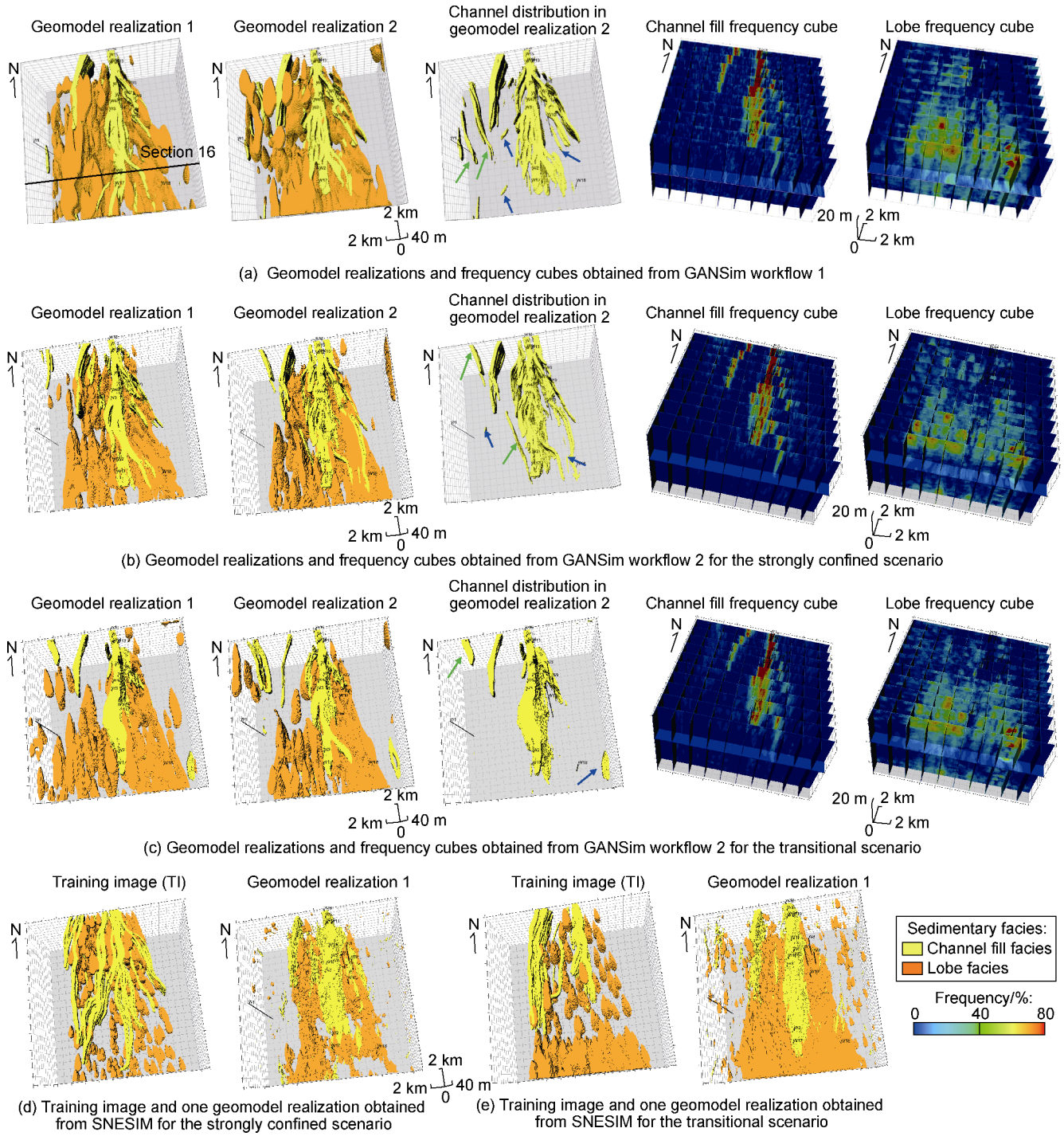

Fig. 7. Turbidite fan geomodel realizations obtained using different modelling methods and the corresponding facies frequency cubes (blue arrows indicate disconnected channel fragments, and green arrows indicate anomalous channel features that are inconsistent with the overall turbidite channel architecture).

with the corresponding input probability cubes, which is confirmed by visual comparisons between the simulated realizations (or calculated frequency cubes) and the input probability cubes in both 3D (Fig. 7 with Fig. 2) and 2D (Fig. 8). This indicates that the input facies probability data exerts a strong conditioning effect on the geomodelling results. The simulation of each realization (400×400×100 cells) takes 0.7 s on one GPU (A100) using the pretrained generator in both workflows.

Regarding the reproduction of expected geological patterns, we can see from the comparison of the simulated realizations with the ground truth facies model or conceptual geomodels (Figs. 2 and 3) that the GANSim results from both workflows are generally realistic in terms of the shape of channels and lobes, the connectivity of channels, the divergent distribution style of channels and lobes along the sedimentary direction (southward), and the cutting relationships between channels and lobes (channels may cut through lobes), although a few disconnected channel fragments appear in regions with

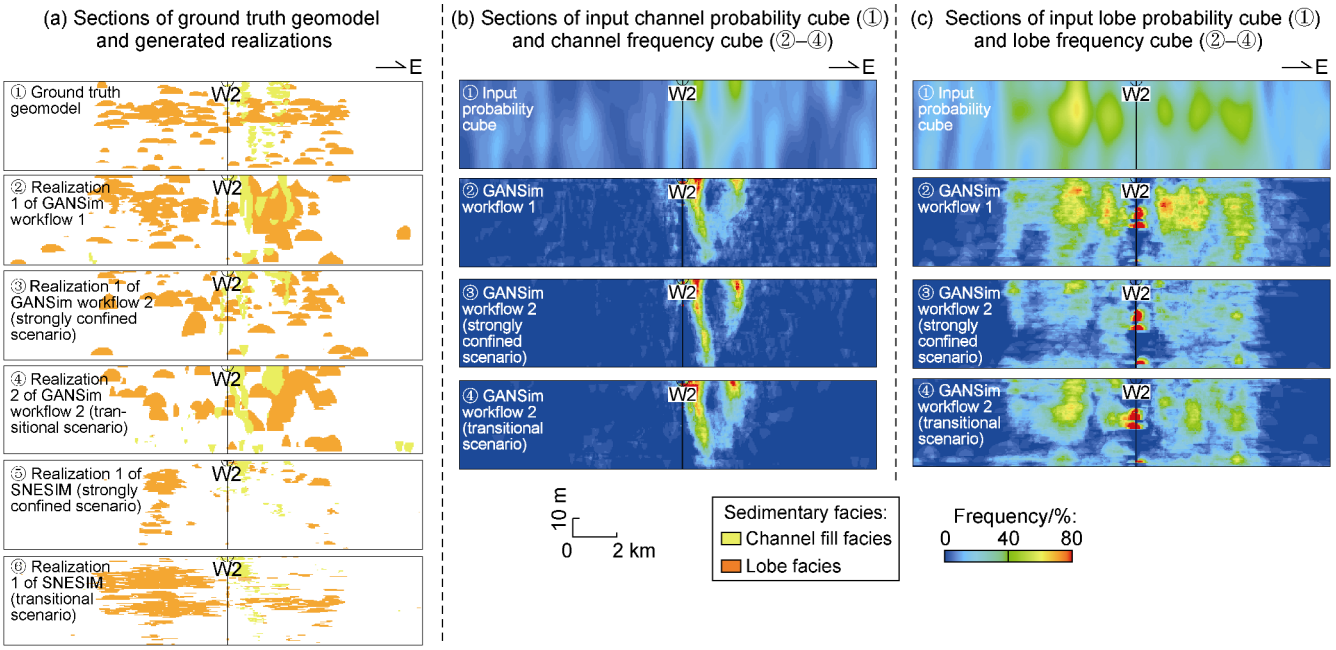

Fig. 8. Comparison among the ground truth geomodel, geomodel realizations and facies frequency cubes obtained using different modelling methods, and the input probability cubes, along section 16 (section location shown in Fig. 7a).

locally higher input channel probabilities, e.g., the channel fragments pointed out by the blue arrows in Fig. 7. In addition, the geomodel realizations from both workflows show large variability, indicating that these realizations of both workflows can effectively represent uncertainty in reservoir prediction.

The channels in all realizations of workflow 1 exhibit near-vertical stacking pattern (Figs. 7 and 8), suggesting either the strongly confined or the transitional scenario. Both GANSim workflows reduce the five prior scenarios to the same two posterior scenarios, indicating that they have the same scenario falsification effect. Such a reduction in scenario uncertainty stems primarily from the conditioning effect of the given data. Additionally, the local discriminator design in GANSim eliminates the disconnection issue around single-pixel well facies data (such disconnections are not observed in realizations), which was a significant limitation in the previous GANSim version [24]. GANSim with a local discriminator design has also been applied to the geomodelling of a field-scale 3D delta reservoir in support of practical CO_2 storage [13]. It achieved the expected geological realism—significantly better than the results obtained using MPS—and demonstrated effective conditioning.

In stationary reservoirs, geological patterns repeat spatially, so GANSim training with cropped conceptual geomodel patches was successful in stationary cases [8]. In non-stationary reservoirs, geological patterns vary across the domain. However, directly training on large conceptual geomodels (each containing the full non-stationary pattern) would be computationally prohibitive. Thus, in this study, we continue to use cropped conceptual geomodel patches for training in both workflows. Although the generator can only learn fragments of the entire non-stationary pattern from cropped patches, when geomodelling with the trained generator for large reservoirs, the conditioning effect of the spatially distributed probability cube serves as a guide to "stitch" the learned pattern fragments into appropriate locations. As a result, the simulated realizations globally present realistic and complete non-stationary patterns, as we can see from Fig. 7. A few pattern fragments are occasionally stitched into unintended locations, e.g., the channels indicated by the green arrows in Fig. 7, which contradict with the globally divergent style and should have been developed in the eastern part of the domain. In addition to conditioning of probability cubes, when global features (e.g., channel direction and facies proportion) are treated as another type of conditioning data, their spatial distributions can also guide the trained generator to produce non-stationary geological patterns [3]. This is similar to the idea in SNESIM where a map of varying affinity and rotation values is taken as a constraint to produce non-stationary geomodels [2].

Figs. 7 and 8 show that the high-value regions in the frequency cubes from both GANSim workflows are more concentrated than in the input probability cubes, indicating a reduced reservoir prediction uncertainty and a mitigation effect for noises in the probability cubes possibly inherited from geophysical data. These effects in uncertainty reduction and noises mitigation mainly result from the integration of geological patterns (e.g., connectivity features and stacking patterns of channels) of the trained generator.

3.2. Comparison of two GANSim workflows

For the majority of modelling results in workflow 1, geological patterns across one realization are consistent, i.e., they belong to one fixed scenario. However, in very few realizations, patterns at different locations may be sampled from different scenarios. For example, in Fig. 9, the channels in the central region of the realization present the characteristics of strongly confined or transitional scenario, but the channels in the west region, indicated by the blue dashed curve in both the 3D geomodel and the 2D section, basically present the characteristics of the valley-confined or weakly confined scenario (i.e., channels are loosely confined), leading to mixed patterns from different scenarios in one geomodel. This occurs because the generator in workflow 1 learns pattern fragments from all scenarios, and during geomodelling, the scenario refinement is based on constraints of conditioning data. Thus, in regions where conditioning effect is weaker (e.g., the western region of the realization in Fig. 9 without any well facies data), pattern fragments from more scenarios may be generated; in contrast, in regions with stronger conditioning effect (e.g., the middle region of the realization in Fig. 9 containing 17 wells), pattern fragments from fewer scenarios may be generated. Such occasional scenario mixing issue is also due to training with cropped patches instead of complete conceptual geomodels. In contrast, workflow 2 avoids the scenario mixing issue since its generator was trained exclusively on a single unfalsified scenario. Indeed, workflow 1 could also train a generator for each of the full scenarios, but this would be too computationally demanding if there are too many scenarios.

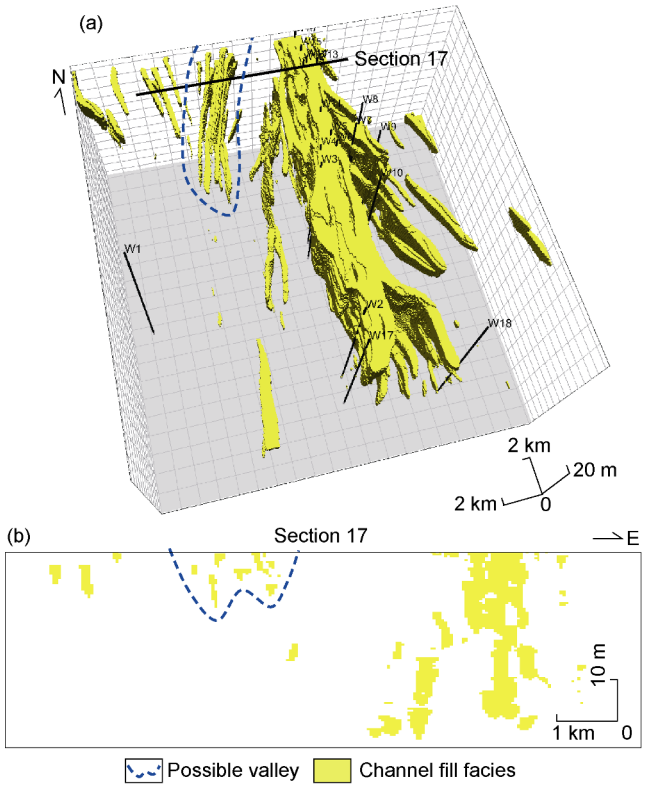

Fig. 9. One facies geomodel realization obtained using GANSim workflow 1 (a) and its cross section (b) (only channel fill facies are displayed).

Besides occasionally generating mixed-scenario geomodels, workflow 1 also requires training data for all scenarios, but once trained, the generator can be used for geomodelling of all scenarios of reservoirs. In comparison, GANSim workflow 2 only requires training data of unfalsified scenarios, but the trained generator can only be used for geomodelling of these specific scenarios. Indeed, a certain number of conceptual geomodels of each scenario (significantly fewer than in workflow 1) are needed for the scenario falsification process in workflow 2, and a sensitive feature filter function for each type of conditioning data is also necessary in this process. If the feature filter funciton fails to adequately constrain the scenario type, many scenarios still persist. In that case, training separate generators for each unfalsified scenario would still be computationally demanding, whereas resorting to a single comprehensive generator of all unfalsified scenarios would reintroduce limitations similar to those in workflow 1.

In addition, from the perspective of probability, workflow 1 expresses a straightforward process of "$P(\boldsymbol{m}) \rightarrow P(\boldsymbol{m}|\boldsymbol{d})$", where $\boldsymbol{m}$ and $\boldsymbol{d}$ refer to geomodel and conditioning data, while workflow 2 can be expressed as "$P(\boldsymbol{m}) \rightarrow P\left[S_k|f(\boldsymbol{d})\right] = P\left[\{\boldsymbol{m}\}_k|f(\boldsymbol{d})\right] \rightarrow P(\boldsymbol{m}|\boldsymbol{d})$", where S_k refers to the k-th scenario and f is a feature filter function. The workflow 2 is a process of cascaded conditioning, with the first subprocess being scenario falsification and the second one being generator conditioning. Note that the unfalsified scenarios from the first subprocess are not necessarily the final scenarios, and an implicit scenario falsification is still involved in the second generator conditioning subprocess. In comparison, scenario falsification is completely fulfilled implicitly in the workflow 1. There may be slight differences between the results of the two workflows, because workflow 1 relies only on well facies data and facies probability cubes interpreted from geophysical data, while workflow 2 also uses the global pattern features from the geophysical data in the initial scenario falsification subprocess.

3.3. Comparison of geomodelling results between GANSim and MPS approaches

We also use an MPS method (i.e., SNESIM in Petrel software) for geomodelling of the reference reservoir, given the conditioning well facies and facies probability cubes. Assuming the geological scenario falsification process is also performed and the strongly confined and transitional scenarios are inferred, we take a random conceptual geomodel of each of the two unfalsified sce-

narios as the training image (TI), along with the conditioning well facies and facies probability cubes, into the SNESIM algorithm to simulate different facies model realizations. The input hyperparameters—e.g., data search parameters, probability weight, and target fraction tolerance—are carefully tuned to produce the most realistic facies models. The TI and one random realization of each scenario are shown in Fig. 7d and 7e. A cross-well section of the realization are shown in Fig. 8a ⑤–⑥ for each scenario.

The SNESIM results are consistent with the conditioning data, as this is inherently designed in the algorithm. However, compared to both GANSim workflows, the SNESIM algorithm is much less effective in reproducing expected geological realism, as shown by the shapes of simulated channels and lobes in GANSim and SNESIM results. Additionally, though the SNESIM algorithm does not require extensive training on GPUs, each realization takes ~10 min on an 8-core i7 laptop, which is nearly 1 000 times slower than geomodelling with the trained generator in GANSim. While GANSim training may require days (less with more computational resources), the trained generator enables rapid geomodelling for arbitrarily large reservoirs with similar geological patterns.

4. Conclusions

This study enhances GANSim geomodelling framework in two aspects. First, two GANSim geomodelling workflows are proposed for reservoirs with multiple possible geological scenarios. Second, to address the reservoir discontinuity problem around wells, a local discriminator architecture is introduced. GANSim workflow 1 aims to train a comprehensive generator neural network applicable to all scenarios for three-dimensional reservoir geomodelling, whereas workflow 2 explicitly introduces a scenario falsification step and trains generators only for unfalsified scenarios.

Taking the geomodelling of a multi-scenario non-stationary turbidite fan reservoir as an example, we evaluate the effectiveness of the enhanced GANSim framework and its reliability for modelling three-dimensional non-stationary reservoirs. The results show that both GANSim workflows can generate multiple realistic geomodel realizations that are consistent with conditioning well facies data and seismic probability cubes. For each workflow, the resulting geomodel realizations exhibit large variability, effectively representing reservoir prediction uncertainty. Despite being trained using cropped conceptual geomodel patches, the generator can still produce complete non-stationary geological architectures in the realizations by leveraging probability cubes as spatial guidance. Both GANSim workflows effectively integrate geological knowledge with diverse conditioning data types. This integration achieves two key outcomes: (1) reduction of scenario uncertainty through conditioning data constraints, and (2) decreased reservoir prediction uncertainty compared to the input probability cubes though learned geological patterns and well facies constraint. The introduction of the local discriminator design successfully eliminates facies disconnection issue around single-pixel well conditioning data in the geomodel realizations. On a single A100 GPU, generating a geomodel realization with 16 million grid cells takes only 0.7 s, further highlighting the good scalability of the enhanced GANSim framework for practical applications. Compared with traditional multipoint geostatistical methods (SNESIM), geomodel realizations generated by enhanced GANSim better honor the expected geological patterns. Although GANSim training is time-consuming and requires large training datasets, once trained, it can be applied to rapid geomodelling of reservoirs of any scale as long as they exhibit similar geological patterns, achieving a modelling speed approximately 1 000 times faster than SNESIM.

Although the generator trained using GANSim workflow 1 can be applied to geomodelling of all scenarios, it may occasionally produce mixed patterns of different scenarios within a single realization. In contrast, workflow 2 avoids this pattern-mixing issue, but it depends on robust scenario falsification, especially a scenario-sensitive feature filter function for each conditioning data type, and the trained generators can only be used for geomodelling of unfalsified scenarios. Workflow 1 considers different scenarios together and may further lead to research on training a large generative AI model for geomodelling across more reservoir types and scales, once the pattern-mixing issue is addressed. However, before such a large AI model is successfully constructed, workflow 2 may still be a good option, as it can produce realistic conditional geomodels for reservoirs of interest while requiring fewer computational resources and less workload. In addition, GANSim requires massive and diverse conceptual geomodels for preparing training datasets, which calls for the development of efficient and automated conceptual geomodel emulation workflows for different reservoir types and scales.

Acknowledgments

We acknowledge the sponsors of the Stanford Center for Earth Resources Forecasting (SCERF). Some of the computing for this project was performed on the Sherlock cluster at Stanford University. We would like to thank Stanford University and the Stanford Research Computing Center for providing computational resources and support that contributed to these research results.

Nomenclature

$\boldsymbol{d}$—reservoir-related observational data;

D—discriminator neural network;

D_0—global discriminator neural network;

D_i—the i-th local discriminator neural network ($1 \le i \le n$);

f—sensitive feature filter function;

G—generator neural network;

I_{wl}—extraction function of well location indicator from well facies data;

K—number of geological scenarios;

L—loss function;

$L_{\boldsymbol{w}}$—conditional loss function for training well facies data;

$L_{\boldsymbol{\pi}}$—conditional loss function for training probability cube data;

$\boldsymbol{m}$—geomodel;

P—probability function;

$p(\boldsymbol{z})$—data distribution of latent vector;

$p(\boldsymbol{x})$—distribution of training facies geomodels;

$p(\boldsymbol{w},\boldsymbol{\pi})$—joint distribution of training well facies data and training probability data;

S_k—the k-th geological scenario ($1 \le k \le K$);

t—a random value in the interval (0, 1);

$\boldsymbol{w}$—training well facies data;

$\boldsymbol{x}$—training facies geomodel data;

$\boldsymbol{x}_G$—generated facies geomodel;

$\hat{\boldsymbol{x}}$—any interpolation between a training facies geomodel and a generated facies geomodel;

$\boldsymbol{z}$—random latent vector;

α_i—weight of the discriminator neural network D_i;

β_1, β_2—weights of $L_{\boldsymbol{w}}$ and $L_{\boldsymbol{\pi}}$;

λ—default weight in the Wasserstein loss with gradient penalty;

$\boldsymbol{\pi}$—training probability cube data;

$\mathbb{E}$—expectation operator.

References

[1] DEUTSCH C V. Geostatistical reservoir modeling. New York: Oxford University Press, 2002.

[2] MARIETHOZ G, CAERS J. Multiple - point geostatistics: Stochastic modeling with training images. Chichester: John Wiley & Sons Inc., 2014.

[3] SONG S H, HUANG J Y, MUKERJI T. Generative geomodelling: Deep learning vs. geostatistics. (2025-06-20)[2025-10-20]. https://doi.org/10.31223/X5B732.

[4] GOODFELLOW I J, POUGET-ABADIE J, MIRZA M, et al. Generative Adversarial Networks. Advances in Neural Information Processing Systems 27. 2014: 10–23.

[5] HO J, JAIN A N, ABBEEL P. Denoising diffusion probabilistic models: LAROCHELLE H, RANZATO M, HADSELL R, et al. Advances in Neural Information Processing Systems 33. Red Hook, NY: Curran Associates, Inc., 2020: 6840–6851.

[6] ZHANG T F, TILKE P, DUPONT E, et al. Generating geologically realistic 3D reservoir facies models using deep learning of sedimentary architecture with generative adversarial networks. Petroleum Science, 2019, 16(3): 541–549.

[7] YANG Z X, CHEN Q Y, CUI Z S, et al. Automatic reconstruction method of 3D geological models based on deep convolutional generative adversarial networks. Computational Geosciences, 2022, 26(5): 1135–1150.

[8] SONG S H, MUKERJI T, HOU J G, et al. GANSim-3D for conditional geomodeling: Theory and field application. Water Resources Research, 2022, 58(7): e2021WR031865.

[9] SONG S H, ZHANG D X, MUKERJI T, et al. GAN-Sim-surrogate: An integrated framework for stochastic conditional geomodelling. Journal of Hydrology, 2023, 620(Part B): 129493.

[10] FAN W Y, LIU G, CHEN Q Y, et al. Geological model automatic reconstruction based on conditioning Wasserstein generative adversarial network with gradient penalty. Earth Science Informatics, 2023, 16(3): 2825–2843.

[11] HU F, WU C L, SHANG J W, et al. Multi-condition controlled sedimentary facies modeling based on generative adversarial network. Computers & Geosciences, 2023, 171: 105290.

[12] CUI Z S, CHEN Q Y, LUO J, et al. Characterizing subsurface structures from hard and soft data with multiple-condition fusion neural network. Water Resources Research, 2024, 60(11): e2024WR038170.

[13] ALQASSAB H M, FENG M, BECKER J A, et al. MAGCS: Machine assisted geologic carbon storage. SPE 222120-MS, 2024.

[14] DI FEDERICO G & DURLOFSKY L J. Latent diffusion models for parameterization of facies-based geomodels and their use in data assimilation. Computers & Geosciences, 2025, 194: 105755.

[15] LEE D, OVANGER O, EIDSVIK J, et al. Latent diffusion model for conditional reservoir facies generation. Computers & Geosciences, 2025, 194: 105750.

[16] XU M H, SONG S H, & MUKERJI T. DiffSim: Denoising diffusion probabilistic models for generative facies geomodeling. International Meeting for Applied Geoscience & Energy, 2024: 1660–1664.

[17] LALOY E, HÉRAULT R, JACQUES D, et al. Training-image based geostatistical inversion using a spatial generative adversarial neural network. Water Resources Research, 2018, 54(1): 381–406.

[18] SONG S H, MUKERJI T, HOU J G. Geological facies modeling based on progressive growing of generative adversarial networks (GANs). Computational Geosciences, 2021, 25(3): 1251–1273.

[19] MO S X, ZABARAS N, SHI X Q, et al. Integration of adversarial autoencoders with residual dense convolutional networks for estimation of non-Gaussian hydraulic conductivities. Water Resources Research, 2020, 56(2): e2019WR026082.

[20] MOSSER L, DUBRULE O, BLUNT M J. Stochastic seismic waveform inversion using generative adversarial networks as a geological prior. Mathematical Geosciences, 2020, 52(1): 53–79.

[21] NESVOLD E, MUKERJI T. Simulation of fluvial patterns

with GANs trained on a data set of satellite imagery. Water Resources Research, 2021, 57(5): e2019WR025787.

[22] BROOKS S, GELMAN A, JONES G L, et al. Handbook of Markov Chain Monte Carlo. Handbook of Markov Chain Monte Carlo. Chance, 2011

[23] CHEN Y & OLIVER D S. Levenberg-Marquardt forms of the iterative ensemble smoother for efficient history matching and uncertainty quantification. Computational Geosciences, 2013.

[24] SONG S H, MUKERJI T, HOU J G. GANSim: Conditional facies simulation using an improved progressive growing of generative adversarial networks (GANs). Mathematical Geosciences, 2021, 53(7): 1413–1444.

[25] SONG S H, MUKERJI T, HOU J G. Bridging the gap between geophysics and geology with generative adversarial networks. IEEE Transactions on Geoscience and Remote Sensing, 2022, 60: 5902411.

[26] HU X, SONG S H, HOU J G, et al. Stochastic modeling of thin mud drapes inside point bar reservoirs with ALLUVSIM-GANSim. Water Resources Research, 2024, 60(6): e2023WR035989.

[27] SONG S H, MUKERJI T, ZHANG D X. Physics-informed multi-grid neural operator: Theory and an application to porous flow simulation. Journal of Computational Physics, 2025, 520: 113438.

[28] WELLNER R, BEAUBOUEF R, VAN WAGONER J, et al. Jet-plume depositional bodies; the primary building blocks of Wax Lake Delta. Transactions - Gulf Coast Association of Geological Societies, 2005, 55: 867–909.

[29] MCHARGUE T R, HODGSON D M, SHELEF E. Architectural diversity of submarine lobate deposits. Frontiers in Earth Science, 2021, 9: 697170.

[30] PYRCZ M J & DEUTSCH C V. Geostatistical Reservoir Modeling (2nd ed.). Oxford University Press, 2014.

[31] POPPER K. The logic of scientific discovery. Scientia, 1959.

[32] SCHEIDT C, LI L, & CAERS J. Quantifying uncertainty in subsurface systems. John Wiley & Sons, 2018.

[33] TARANTOLA A. Popper, Bayes and the inverse problem. Nature Physics, 2006.

[34] BORG I, GROENEN P J F. Modern multidimensional scaling: Theory and applications. 2nd ed. New York: Springer, 2005.

[35] SCHEIDT C, TAHMASEBI P, PONTIGGIA M, et al. Updating joint uncertainty in trend and depositional scenario for reservoir exploration and early appraisal. Computational Geosciences, 2015, 19(4): 805–820.

[36] PARK H, SCHEIDT C, FENWICK D, et al. History matching and uncertainty quantification of facies models with multiple geological interpretations. Computational Geosciences, 2013, 17(4): 609–621.

[37] SCHEIDT C, JEONG C, MUKERJI T, et al. Probabilistic falsification of prior geologic uncertainty with seismic amplitude data: Application to a turbidite reservoir case. Geophysics, 2015, 80(5): M89–M12.

[38] HERMANS T, CAERS J, & NGUYEN F. Assessing the probability of training image-based geological scenarios using geophysical data. Lecture Notes in Earth System Sciences, 2014.

[39] TAN X, TAHMASEBI P, & CAERS J. Comparing training-image based algorithms using an analysis of distance. Mathematical Geosciences, 2014.

[40] JOURNEL A G. Combining knowledge from diverse sources: An alternative to traditional data independence hypotheses. Mathematical Geology, 2002, 34(5): 573–596.

[41] WEI X L, YIN Z, SCHEIDT C, et al. Constructing priors for geophysical inversions constrained by surface and borehole geochemistry. Surveys in Geophysics, 2024, 45(4): 1047-1079.

[42] GULRAJANI I, AHMED F, ARJOVSKY M, et al. Improved training of Wasserstein GANs: VON LUXBURG U, GUYON I, BENGIO S, et al. Proceedings of the 31st International Conference on Neural Information Processing Systems. Red Hook, NY: Curran Associates Inc., 2017: 5769–5779.

[43] DEPTUCK M E, SYLVESTER Z, PIRMEZ C, et al. Migration-aggradation history and 3-D seismic geomorphology of submarine channels in the Pleistocene Benin-major Canyon, western Niger Delta slope. Marine and Petroleum Geology, 2007, 24(6/7/8/9): 406–433.

[44] MCHARGUE T, PYRCZ M J, SULLIVAN M D, et al. Architecture of turbidite channel systems on the continental slope: Patterns and predictions. Marine and Petroleum Geology, 2011, 28(3): 728–743.

[45] AVSETH P, MUKERJI T, MAVKO G. Quantitative seismic interpretation: Applying rock physics tools to reduce interpretation risk. Cambridge: Cambridge University Press, 2005.

[46] KARRAS T, AILA T, LAINE S, et al. Progressive growing of GANs for improved quality, stability, and variation. arXiv Preprint, 2017, arXiv: 1710.10196.

[47] KINGMA D P, BA J. Adam: A method for stochastic optimization. (2014-12-22)[2025-11-12]. https://doi.org/10.48550/arXiv.1412.6980.